Anisotropic In-Plane Phonon Transport in Silicon Membranes Guided by Nanoscale Surface Resonators

Sanghamitra Neogi[1,*] and Davide Donadio[2]

[1]*Ann and H.J. Smead Aerospace Engineering Sciences, University of Colorado Boulder, Boulder, Colorado 80303, USA*
[2]*Department of Chemistry, University of California Davis, One Shields Avenue, Davis, California 95616, USA,*

Anisotropic phonon transport is observed along different lattice directions in two-dimensional (2D) and layered materials. However, this effect vanishes in homogeneous, covalently bonded films, as the thickness is increased beyond few atomic layers. Here we establish a fundamental mechanism to induce anisotropic phonon transport in quasi-2D materials with in-plane isotropic symmetry. The anisotropy is engendered by the resonant modes of surface nanostructures that hybridize with membrane modes. Using atomistic lattice dynamics and classical molecular dynamics we demonstrate that the thermal conductivity of silicon membranes with surface nanofins is larger by approximately 100% parallel to the fins than in the perpendicular direction. The primary advantage of these configurations is that they would be technologically viable for implementation to existing and innovative material architectures. We anticipate that our results will open up alternative research directions to control phonons of technology-enabling nanomaterials for a broad range of applications, including thermal management in three-dimensional interconnected nanoelectronics, thermoelectric conversion to IR sensing.

I. INTRODUCTION

Heat conduction in bulk materials is well described by Fourier's law [1] in terms of the proportionality between the heat current and the local temperature gradient. The coefficient of proportionality defines the thermal conductivity, κ: an intensive property, independent of material dimension and geometry. However, recent works heightened the debate over the applicability of Fourier's law to describe heat conduction in low-dimensional materials [2–4]. In fact the thermal conductivity (TC) of materials at the nanoscale can differ significantly from their bulk counterparts [5–12], with major consequences for the application of low-dimensional materials, such as graphene [6–8,13,14], transition metal dichalcogenides [15–17], nanotubes [9], and nanowires [11,12], in electronic, optoelectronic, and phononic and/or thermal devices [15,18–24,26].

Dimensionality reduction significantly affects lattice thermal transport, even violating Fourier's law. For example, TCs of one- and two-dimensional nanostructures exhibit anomalous size dependence [8,9,27,28], and TCs of nanowires and nanomembranes show an enhanced sensitivity on surface features [29,30]. Anisotropic in-plane TC manifests itself in two-dimensional materials, such as

few-layer black phosphorus [31], and has been theoretically predicted for phosphorene [32], borophane (hydrogenated boron sheet) [33], arsenene [34], and silicene [35]. The anisotropy emerges as a consequence of differing bonding environments along the zigzag and the armchair lattice directions in these materials. Surface reconstructions are also shown to create in-plane TC anisotropy in two-four atomic-layer-thick silicene, with the effect monotonically decreasing with increasing thickness [35]. In bulk materials, TC anisotropy stems from the varied bonding environment. For example, strong anisotropy between the in-plane and the cross-plane directions occurs in van der Waals layered materials due to chemical bonding [7,36,37], or in-plane anisotropy arises in nanoporous thin films due to anisotropic pore spacing [38]. To date, however, in-plane anisotropic thermal conductivity has not been reported for single-crystal thin films of materials with isotropic bond symmetry, e.g., cubic or hexagonal.

In this article, we introduce a physical mechanism to engender anisotropic in-plane phonon transport in thin films and membranes of isotropic materials. Such an anisotropy, which can exceed by a ratio of 2 between the parallel and perpendicular components of TC, is introduced by exploiting the hybridization of membrane phonon modes with the resonant modes of surface nanostructures. Using atomistic lattice dynamics and classical molecular dynamics simulations we illustrate that phonon

---

*sanghamitra.neogi@colorado.edu

propagation in suspended silicon membranes (> 20 atomic layers) with surface "fins" is anisotropic and guided by the fin geometry. We demonstrate the concept on silicon membranes with periodic surface nanoscale pillars and fins. Silicon is chosen because of its wide use in a broad range of technological applications and the ease of fabrication, however the concept is applicable to other materials.

In recent years, the effect of dimensionality reduction [29,30,39–46] and surface roughness, due to oxidation [30, 44,47], amorphization [29,39,40], or engineered nanostructures [41–43,45,46] have been extensively discussed as strategies to reduce TC of silicon, yielding potential thermoelectric applications [48,49]. In particular, nanopillar resonators on silicon thin films have been illustrated to exhibit unique subwavelength phonon properties at the nanoscale, resulting in strong κ reduction [42,46]. Whereas former works focused on TC reduction in either thin-film-based phononic crystals or metamaterials, our simulations unveil *a fundamental mechanism to tune phonon propagation direction and localization, and, as a result, the directionality of heat transport in thin films*, using nano-engineered surfaces. While we also observe an overall TC reduction, here we primarily discuss the microscopic origin of the anisotropic in-plane phonon transport induced by surface nanoscale resonators, using a recently developed unified theory of thermal transport in crystalline and disordered solids [50].

II. METHODS AND MODELS

Representative atomistic model configurations of suspended silicon (Si) membranes with surface nanoscale (a) pillars and (b) fins are shown in Fig. 1 (inset). We prepare the membrane configurations by cleaving bulk Si supercells along the [001] direction to construct membranes with pristine surfaces as well as membranes with monolithic pillars and fins at both surfaces. The supercells are constructed by replicating a Si cubic conventional cell (CC): the pristine membrane supercells consist of $8 \times 8 \times n_z$ CCs, the monolithic surface nanopillars $4 \times 4 \times 2$ CCs, and nanofins $4 \times 8 \times 2$ CCs, respectively, where n_z is the number of unit cells in the z direction. We investigate single-crystalline membranes with four different thicknesses: 3, 5, 10, and 20 nm, with $n_z = 6, 10, 20$, and 37, respectively. Both the surfaces of the pristine and the structured membranes are 2×1 reconstructed forming rows of dimers [51], to minimize the number of dangling bonds. The supercells are heated to 1500 K for 2 ns and then quenched to 300 K by Langevin dynamics with a cooling rate of approximately 10^{11} K/s to obtain equilibrated configurations. The surface nanopatterns relax into periodic features with spacing 2 nm, height 1 nm. and area 2.1×2.1 nm^2 (pillars) or $2.1 \times$(sample length) nm^2 (fins), respectively.
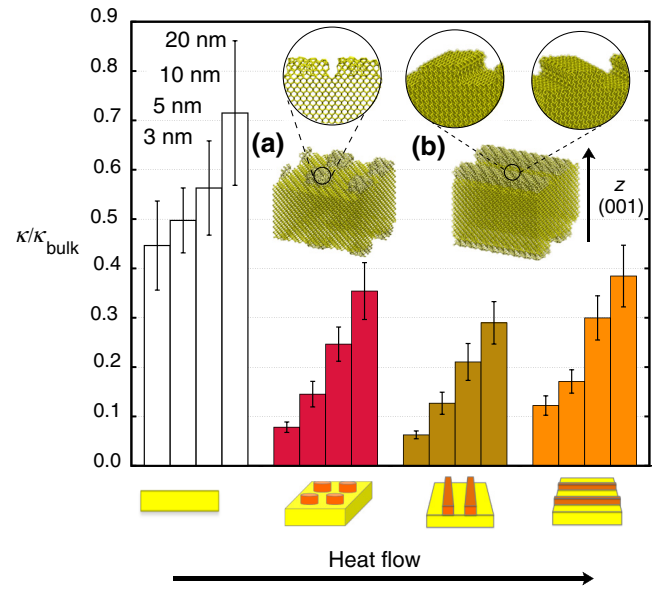

FIG. 1. Ratio between the room-temperature thermal conductivity of bulk silicon and silicon membranes ($\kappa/\kappa_{\mathrm{Bulk}}$) with atomistic smooth surfaces (white), surface nanoscale pillars (red) and fins (gold, orange) with thicknesses 3, 5, 10, and 20 nm, respectively. Cartoons (bottom) refer to the corresponding configurations above them. The κ values represent the in-plane κ tensor components along the arrow direction shown at the bottom of the figure. The results illustrate the anisotropy of the in-plane κ as a function of the fin orientation. (Inset) Representative microscopic configurations of the membranes with nanoscale (a) pillars, (b) fins at the top and the bottom surfaces.

In order to gain microscopic understanding of heat transport in the nanostructured membranes, we perform equilibrium molecular dynamics (EMD) simulations, in which the interatomic interactions are modelled using the empirical Tersoff potential [52] (see details [53]). Although more accurate machine-learning models are now available, [54, 55] and even though the Tersoff potential overestimates the bulk TC of crystalline silicon, it provides an excellent compromise between performance and transferability. In fact, it reproduces well the TCs of amorphous silicon [50,56] and, most importantly, the changes in TC induced by nanostructuring and surface engineering [30,39,43]. The EMD simulations are carried out using LAMMPS [57]. The TC is computed from the fluctuations of the heat current in the EMD simulations, using the Green-Kubo relation [58–60]. We verify that a X-Y periodic cell dimension of $16 \times 16 \times n_z$ CCs ($8.7 \times 8.7 \times$ thickness nm^3), is sufficient to achieve well converged values of κ [43], by comparing results with cells as large as $64 \times 64 \times n_z$ CCs ($34.8 \times 34.8 \times$ thickness nm^3). We then perform a spectral analysis of the heat-carrying vibrations of the membranes and computed modal contributions to κ, implementing a lattice-dynamics-based quasiharmonic Green-Kubo (QHGK) approach [50], which naturally bridges the

Allen and Feldman model for heat transport in glasses [61] and the phonon Boltzmann transport theory for crystals [62]. We adopt a perturbative approach to compute the three-phonon scattering rates, and neglect contributions from four or higher-order scattering processes. The supercells used in the lattice dynamics calculations are pristine membranes with $8 \times 8 \times 6$ CCs containing 3072 atoms, and membranes with 1-nm-high pillars (2.1 nm $\times$ 2.1 nm lateral dimension) and fins (2.1 nm thickness) containing 3584 and 4160 atoms, respectively. All calculations refer to systems at room temperature (300 K).

III. RESULTS AND DISCUSSION

Figure 1 summarizes the in-plane κ of nanopatterned membranes computed from EMD with the Green-Kubo relation. The κ values are scaled with respect to the bulk Si reference: $\kappa_{bulk} = 197 \pm 20$ W/m-k [56]. The presence of surface nanostructures significantly reduces TCs (red, gold, and orange blocks) compared to pristine membranes (white blocks) of similar thicknesses, confirming the trend reported in the literature [30,42–46,63]. Former works showed that localized resonant modes of the nanopillars hybridize with the underlying phonon dispersions of the base Si membranes and such couplings, in combination with surface scattering, drastically lower the in-plane TC [30,42,43]. For a given shape and size of the surface nanostructure, the reduction of κ increases with decreasing membrane thickness. In our study, κ drops by a maximum of 13-fold and 16-fold for the 3-nm-thick membranes with nanopillars and fins, respectively. The reduction factor is approximately 3 for the 20-nm-thick membranes. The reduction of κ with decreasing membrane or thin-film thickness is attributed to the increase of the surface-to-volume ratio and consequentially, the enhancement of mode coupling between the membrane and the resonators [43,45]. Whereas we observe similar trends, our results are in stark contrast with former simulations that predict κ reduction of about 2 orders of magnitude [46]. These discrepancies may arise either from the differences in the equilibrated structures of the nanopillared membranes, or from the differences in the protocol how EMD simulations are carried out (e.g., how size and time convergence issues are addressed in the EMD simulations). Remarkably, as opposed to pillars, which reduce κ homogeneously, the nanofins break the membrane X-Y in-plane symmetry engendering strongly anisotropic TC. The TC parallel to the nanofins ($\kappa_\parallel$) is much higher than in the perpendicular direction ($\kappa_\perp$) (Fig. 1). $\kappa_\parallel$ exceeds $\kappa_\perp$ by $\sim 100\%$ in the 3-nm and $> 30\%$ in the 20-nm-thick membranes.

Hereafter, we aim at unraveling the microscopic origin of the observed anisotropic thermal conductivity, and its relation to the phonon localization and hybridization due to
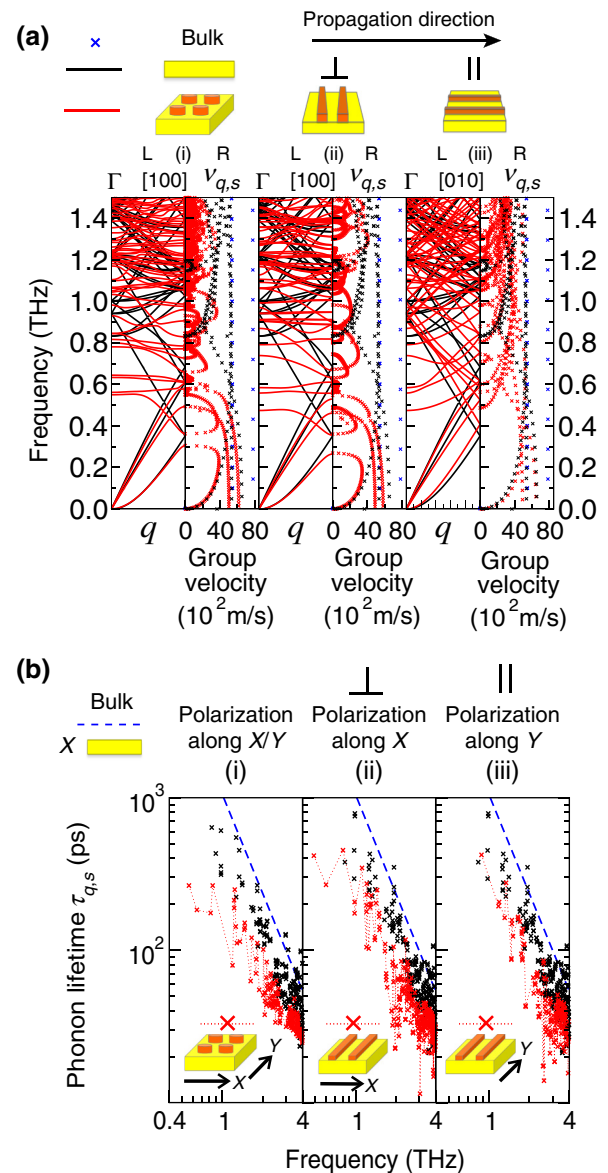

FIG. 2. Spectral analysis of phonon propagation in nanostructured 3-nm-thick silicon membranes: (a) Phonon dispersion (L) and group velocities (R) in membranes with periodic nanoscale surface (i) pillars and (ii, iii) fins, calculated within the harmonic approximation along different symmetry directions. Cartoons on top of the figure represent the corresponding geometries. The in-plane phonon properties are shown along (ii) perpendicular ($\perp$) and (iii) parallel ($\parallel$) to the fins in the membranes with nanofins. The black and red lines in the L panels represent pristine and nanostructured membranes, respectively. The flattening of modes due to resonances can be clearly discerned in the two L panels [(i), (ii)] while "guide"like modes are visible in (iii). The blue, black, and red X's in R panels represent bulk Si, pristine, and nanopatterned membranes, respectively. The R panels reflect the direct effect of phonon hybridization on group velocities. (b) Phonon lifetimes in membranes with (i) pillars and (ii, iii) fins, calculated with anharmonic lattice dynamics. Blue dashed lines indicate the fitting of τ of bulk silicon to $1/\omega^2$. The signatures of anisotropic phonon properties are manifested in the $\perp$ and $\parallel$ panels.
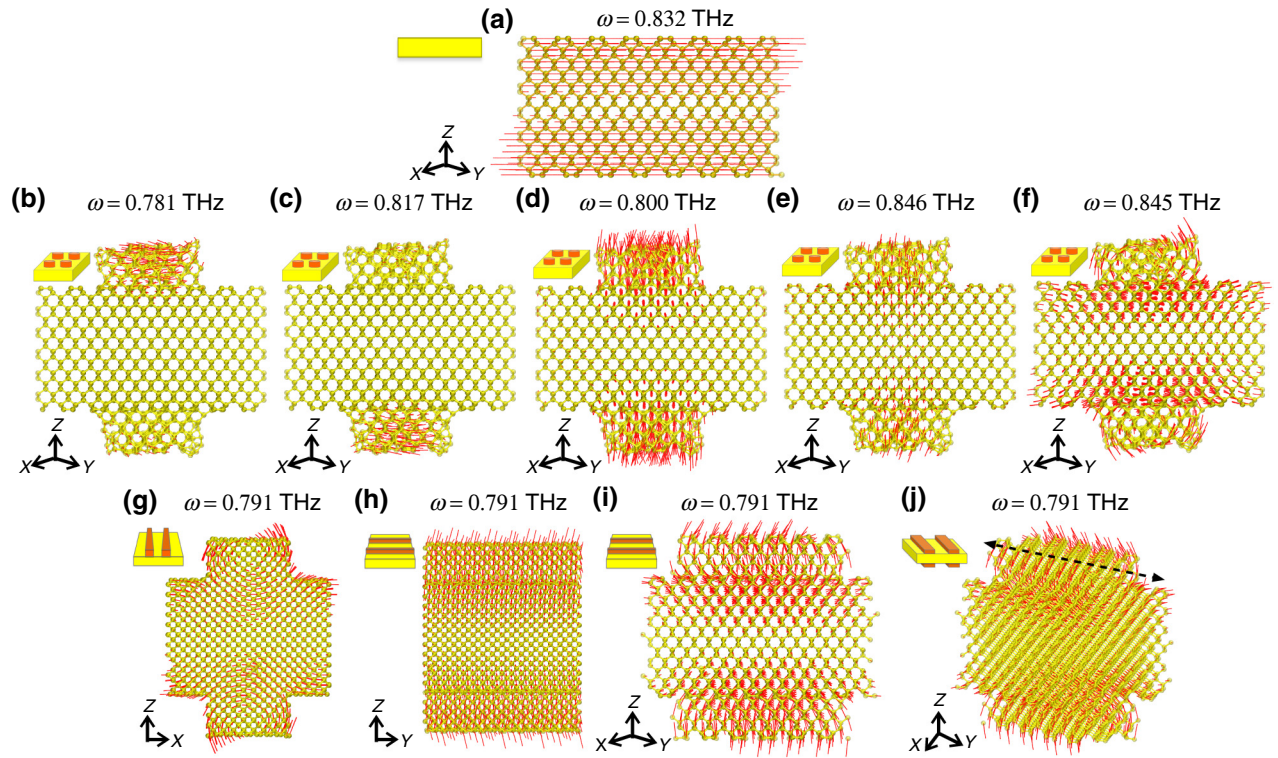
FIG. 3. Phonon-mode hybridization in nanostructured membranes. (a) Polarization vector of the membrane mode with frequency approximately 0.8 THz, corresponding to wavevectors at the Γ point. Red lines represent the projection of the eigenvector $\hat{e}_n(i)$ of mode i on the coordinates of atom n. Here $i \equiv (\mathbf{q}, s)$. (b)–(f) Polarization of the membrane modes, which hybridize with the resonances of the surface nanopillars, leading to modes localized at the pillar and reduced displacements of the core atoms. (g)–(j) Hybridization of the membrane mode with resonances of the surface nanofin, leading to anisotropic displacement patterns in the perpendicular (g) and parallel (h) to the fin direction. (i)–(j) Alternative views of the "guide"like modes of the membrane with nanofins.

the presence of the surface resonators. To this end, we perform a detailed spectral analysis using anharmonic lattice dynamics and the QHGK approach. We highlight the low-frequency phonons, below 1.5 THz, since they provide the dominant contribution to TC, thus elucidating the trends exhibited in Fig. 1. Both $\omega_s(\mathbf{q})$ and $\mathbf{v}_{\mathbf{q},s}$, shown in Fig. 2(a), display the evidences of hybridization of the propagating membrane phonons with the surface nanostructure resonances. The comparison between the dispersion of modes of the pristine (black) and the nanostructured membranes (red) [Fig. 2(a) (i-L)] reveals that the surface nanopillar introduces numerous resonances that hybridize with the membrane modes, leading to the appearance of multiple flat branches in the dispersion diagram. The polarization vectors of these flat modes are significantly modified due to hybridization [44,45]. In Fig. 3 we show the polarization vectors, corresponding to wavevectors at the Γ point, of a representative membrane mode with frequency approximately 0.8 THz [Fig. 3(a)], and of the hybridized modes at similar frequencies in nanostructured membranes [Figs. 3(b)–3(j)] (also at Γ point). Figure 3(a) shows the polarization vector of the TA mode of the membrane, which involves participation of all atoms. In comparison,

the flat branches are fully or partially localized in the nanopillars [Figs. 3(b)–3(f)], with reduced participation from the membrane core atoms, indicating hybridization and localization. Flat modes also appear in the dispersion diagram of the membranes with nanofins, for $\mathbf{q}$ propagation vector perpendicular to the fins [Fig. 2(a) (ii-L)] (hereafter will be referred to as $\perp$ modes), with reduced participation from atoms belonging to the core of the membrane [Fig. 3(g)]. Remarkably, the dispersion relations parallel to the fins do not exhibit flat modes, but rather the presence of "guide"like modes [Fig. 2(a) (iii-L)] [64](referred to as $\parallel$ modes), with extended participation of both the fin and the membrane atoms [Figs. 3(h)–3(j)]. Acoustic phonon dispersions at small frequencies (approximately 0.4 THz) or wavevectors are not affected by surface features, as revealed across the panels representing different cases in Fig. 2. However, the lowest frequency of the flat phonon branches could possibly be tuned by altering the dimensions of the surface nanoscale patterns [45].

The mode flattening has a direct influence on the phonon group velocities ($\mathbf{v}_{\mathbf{q},s} = d\omega_s/d\mathbf{q}$); they are significantly smaller in nanostructured membranes than in the pristine
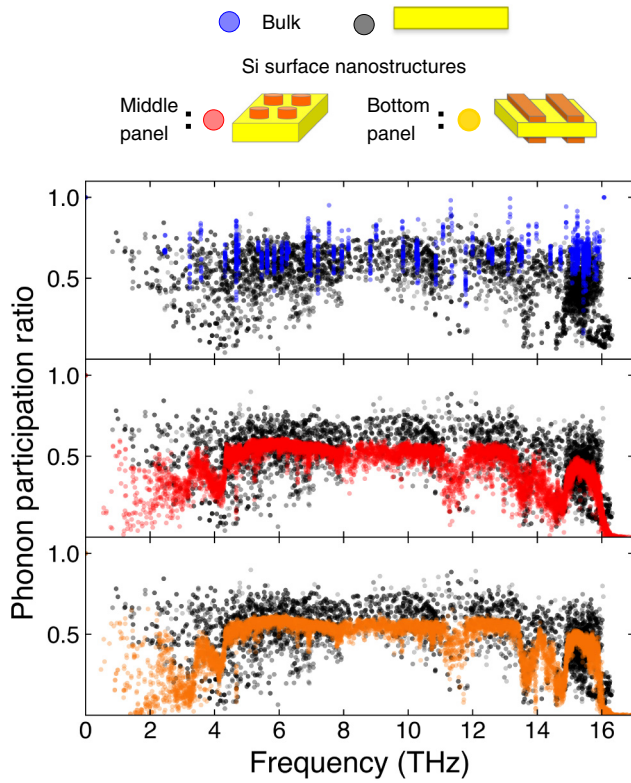
FIG. 4. Participation ratio (p_i) of phonons of nanostructured silicon membranes: surface nanostructures are instrumental in localizing phonon modes, especially in the low-frequency region. p_i indicates the fraction of atoms participating in a given eigenmode and is defined as $p_i^{-1} = N \sum_n [\sum_\alpha e_{\alpha,n}^*(i) e_{\alpha,n}(i)]^2$, where $e_{\alpha,n}(i)$ is the α component of the mode i relative to the coordinate of the atom n.

membrane [Fig. 2(a)-R] panels, and Fig. S1 within the Supplemental Material [65]). Such a reduction of $\mathbf{v}_{\mathbf{q},s}$ is the main cause for the TC reduction in pillared membranes, and along the direction perpendicular to the fins (along [100]) in membranes with nanofins. In both the cases $\mathbf{v}_{\mathbf{q},s}$'s are drastically reduced at the frequencies where the surface resonances couple with the membrane phonon modes [Fig. 2(a) (i-R) and (ii-R)], and result in flat branches. In contrast, $\mathbf{v}_{\mathbf{q},s}$ of ∥ modes (along [010]), remain significantly larger (iii-R). This aspect reveals the advantage of the fin geometry to induce anisotropy, and offers insight to guide phonon propagation in quasi-2D materials by exploiting surface nanostructure geometry.

The altered dispersions also impact the phonon relaxation times ($\tau_{\mathbf{q},s}$) in nanostructured membranes [Fig. 2(b) and Fig. S2 within the Supplemetal Material [65]]. For bulk Si, $\tau_{\mathbf{q},s}$ diverges for frequency tending to zero as $1/\omega^\alpha$, with $\alpha \sim 2$ (blue) [66], whereas for pristine membranes $\tau_{\mathbf{q},s}$ exhibits a slightly weaker divergence, $\alpha \sim 1.5$ (black). In comparison, phonon lifetimes are considerably lower in nanopatterned membranes than in pristine membranes

at low frequencies (≤ 3 THz). An even more remarkable impact of resonances can be noted when we sort $\tau_{\mathbf{q},s}$ according to phonon main polarization direction. We identify the main polarization direction from the maximum projection of the eigenvectors [$e_{\alpha,n}(i)$] of the dynamical matrix along the three Cartesian axes, α [Fig. 2(b)]. Here n denotes atoms and $i \equiv (\mathbf{q}, s)$. The $\tau_{\mathbf{q},s}$'s of low-frequency phonons, mainly polarized in plane, show identical behavior (along X or Y) in the nanopillared membrane, and reach a plateau (≤ 1 THz) [Fig. 2(b)(i)]. However, the low-frequency ∥ modes, are long-lived while $\tau_{\mathbf{q},s}$ of the ⊥ modes reach a plateau [Fig. 2(b)(ii) and (iii)]. This suggests that mode hybridization not only affects $\mathbf{v}_{\mathbf{q},s}$ but impacts the phonon-phonon scattering processes as well. In fact, the additional surface modes provide a larger number of three-phonon scattering channels that satisfy energy and quasimomentum conservation [67], which reflects in higher overall scattering rates and lower lifetimes. Such enhancement of the three-phonon scattering phase space is more efficient in reducing phonon lifetimes when the surface modes are flat, i.e., either in nanopillared membranes or for propagation perpendicular to the fins. The $\tau_{\mathbf{q},s}$'s of higher-frequency phonon modes are not affected significantly. A similar observation is reported for oxidized silicon membranes that native oxide at surfaces induces resonances to strongly suppress the phonon mean-free paths below 4 THz [44].

As we illustrate earlier, resonance hybridization alters the propagation character of vibrational modes in nanostructured membranes. Figure 4 shows the participation ratio [68] of the vibrational modes of the membranes with and without surface nanostructures. Surface reconstruction does not impact significantly the extended nature of the phonons of the pristine membrane [top, Fig. 3(a)], other than localizing some modes near the surfaces both in the high-frequency (> 14 THz) and in the 4–6 THz range. In the nanostructured membranes, the latter modes are extended to engage the surface nanostructures, resulting in higher participation. However, the most striking impact of resonance hybridizations can be observed in the reduced participation ratio of the low-frequency phonon modes ($\omega \leq 2$ THz), reflecting the localized nonpropagating character of these modes [Fig. 4 (middle and bottom), Figs. 3(b)–3(j)]. Most of these modes can be categorized as "diffusons," with approximately 0 group velocity but still extended to significant portion of the membrane model, and few of them are fully localized ("locons") [68]. Note that the participation ratio is not resolved with respect to the propagation direction and thus it does not offer any information regarding anisotropic transport. In recent years, remarkable evidences of phonon localization have been demonstrated in nanostructured materials due to the introduction of multiple scattering and interference mechanisms with periodicity on the order of the length scale of the propagating waves [69–73]. Our calculations
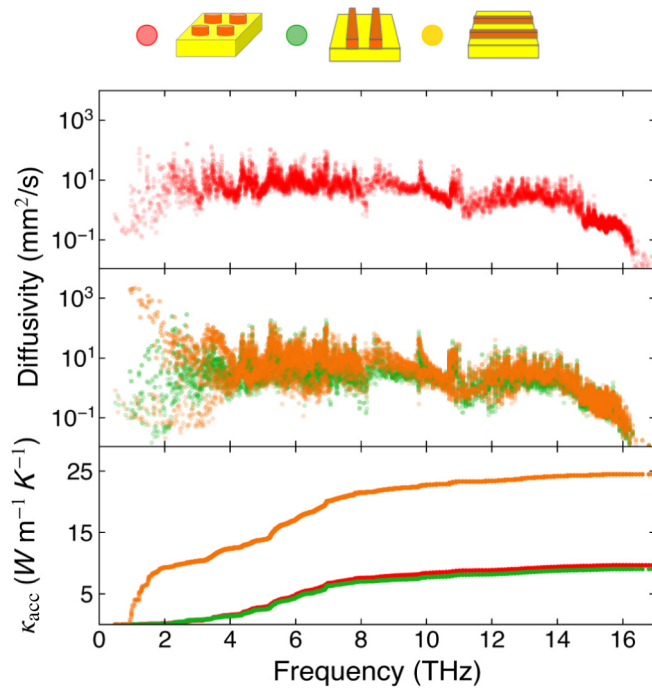
FIG. 5. Diffusivity of vibrational modes of membranes with periodic nanoscale surface (a) pillars (red) and (b) fins [⊥ (green), ∥ (orange)], calculated within the quasi-harmonic Green-Kubo approach. (c) Thermal conductivity accumulation function of nanostructures membranes. Both (b) and (c) panels exhibit anisotropic phonon properties.

suggest that localization can be induced through surface resonances, without introducing internal scatterers within the material. Surface nanostructures induce numerous resonances, each of which may hybridize with the host phonons, and thus enable the emergence of unique localization, thus engendering "glasslike" phonon transport, and turning the host membrane or film into a "phonon-glass" for low-frequency modes.

The hybridized vibrational modes are localized and nonpropagating with approximately 0 group velocity, however, they may have finite diffusivity, and thus carry heat [61,74,75]. We computed the mode-resolved TC of the nanostructured membranes by QHGK. The TC contribution of each mode i with frequency ω can be expressed as $\kappa_i^\alpha(\omega) = c_i D_i^\alpha$, where α is the direction of propagation (we consider only the diagonal elements of κ), c_i the modal heat capacity per unit volume of each state i and D_i is the mode diffusivity, $D_i^\alpha = \sum_j (v_{ij}^\alpha)^2 \tau_{ij}$. v_{ij}^α and τ_{ij} are generalized velocities and generalized phonon lifetimes, as defined in Ref. [50]. The diffusivity of the vibrational modes of the nanostructured membranes at lower frequencies, $\omega \lesssim 4$ THz exhibits clear signatures of resonance hybridization (Fig. 5): D_i of the modes of nanopillared membranes and the ⊥ modes in the membranes with fins are orders of magnitude lower than the ∥ modes. Low

D_i values indicate the "glassy" nature of the vibrational modes engendered by surface resonances, and it is a consequence of the localization displayed in Fig. 4. Particularly remarkable is the anisotropic nature of phonon diffusivity in the membranes with nanofins: a number of ∥ modes retain a propagating phonon character with D_i exceeding 10^3 mm²/s at low frequency, whereas the ⊥ modes have mostly diffusive character with lower values of D_i at low frequency. In the lower panel of Fig. 5, we integrate the contribution from all phonons up to a frequency ω to obtain the frequency-dependent TC accumulation function [$\kappa_{\text{acc}}(\omega)$]. The integrated values of κ_{acc} to the end of the spectrum is in excellent agreement with the EMD results (Fig. 1). The accumulation function shows that the origin of the strong TC anisotropy observed for the membranes with fins mostly originates from the low frequency "guidelike" ∥ modes with propagating phonon character and high diffusivity. In turn, there is no substantial difference between the heat carriers ⊥ to the fins and those in nanopillared membranes.

IV. CONCLUSION

In conclusion, we establish that anisotropic surface nanostructures can engender directional mode propagation, and therefore anisotropic TC, in otherwise isotropic membranes or films. The modal propagation is guided by resonance hybridization induced by surface nanostructures. We demonstrate this mechanism by analyzing phonon properties of ultrathin silicon membranes with periodic nanoscale pillars and fins on their surfaces. Localized, nonpropagating modes with flat dispersion relations appear across the whole frequency spectrum in nanopillared membranes. Similar bands exist in membranes with fins, in the direction perpendicular to the fins. As a consequence, group velocities are strongly reduced in these cases. Remarkably, "guide"like modes appear parallel to the fins, resulting in less reduction of group velocities. The lifetimes of low-frequency modes reach a plateau in the pillar and across-fin directions, and they have low thermal diffusivity. While modes in the parallel-fin direction show weak divergence and reveal onset of ballistic propagation, mostly retaining propagating character. The thermal conductivities computed with EMD and QHGK approaches reflect the reduction and the anisotropy. $\kappa_\parallel$ exceeds $\kappa_\perp$ by approximately 100% in 3 nm and >30% in the 20-nm-thick membranes. Our results establish the physical mechanism to localize and guide phonons of quasi-2D materials using surface nanoscale engineering.

The primary advantage of these configurations is that they will be technologically viable for implementation in existing devices and innovative material architectures. The periodic nanopillars or fins could be fabricated using dry etching [76], metal-assisted chemical (wet) etching [77], dislocation-driven mechanism [78], and vapor-liquid-solid

processes [79,80]. We anticipate that our results showing direct relationship between engineered nanoscale surface resonators and phonons will open up alternative research directions to control phonons of existing and alternative technology-enabling nanomaterials for a broad range of applications, including thermal management in nanoelectronics, thermoelectric conversion to IR sensing.

ACKNOWLEDGMENTS

[1] J. B. J. Fourier, *Théorie Analytique de la Chaleur* (F. Didot, Paris, 1822).

[2] S. Lepri, R. Livi, and A. Politi, Thermal conduction in classical low-dimensional lattices, Phys. Rep. **377**, 1 (2003).

[3] A. Dhar, Heat transport in low-dimensional systems, Adv. Phys. **57**, 457 (2008).

[4] M. Simoncelli, N. Marzari, and A. Cepellotti, Generalization of Fourier's Law Into Viscous Heat Equations, Phys. Rev. X **10**, 011019 (2020).

[5] S. Liu, X. Xu, R. Xie, G. Zhang, and B. Li, Anomalous heat conduction and anomalous diffusion in low dimensional nanoscale systems, Eur. Phys. J. B **85**, 337 (2012).

[6] S. Ghosh, W. Bao, D. L. Nika, S. Subrina, E. P. Pokatilov, C. N. Lau, and A. A. Balandin, Dimensional crossover of thermal transport in few-layer graphene, Nat. Mater. **9**, 555 (2010).

[7] A. A. Balandin, Thermal properties of graphene and nanostructured carbon materials, Nat. Mater. **10**, 569 (2011).

[8] X. Xu, L. F. Pereira, Y. Wang, J. Wu, K. Zhang, X. Zhao, S. Bae, C. T. Bui, R. Xie, J. T. Thong *et al.*, Length-dependent thermal conductivity in suspended single-layer graphene, Nat. Commun. **5**, 3689 (2014).

[9] C.-W. Chang, D. Okawa, H. Garcia, A. Majumdar, and A. Zettl, Breakdown of Fourier's Law in Nanotube Thermal Conductors, Phys. Rev. Lett. **101**, 075903 (2008).

[10] T. Meier, F. Menges, P. Nirmalraj, H. Hölscher, H. Riel, and B. Gotsmann, Length-Dependent Thermal Transport along Molecular Chains, Phys. Rev. Lett. **113**, 060801 (2014).

[11] T.-K. Hsiao, H.-K. Chang, S.-C. Liou, M.-W. Chu, S.-C. Lee, and C.-W. Chang, Observation of room-temperature ballistic thermal conduction persisting over 8.3 μm in sige nanowires, Nat. Nanotech. **8**, 534 (2013).

[12] N. Yang, G. Zhang, and B. Li, Violation of Fourier's law and anomalous heat diffusion in silicon nanowires, Nano Today **5**, 85 (2010).

[13] d. Ghosh, I. Calizo, D. Teweldebrhan, E. P. Pokatilov, D. L. Nika, A. A. Balandin, W. Bao, F. Miao, and C. N. Lau, Extremely high thermal conductivity of graphene: Prospects for thermal management applications in nano-electronic circuits, Appl. Phys. Lett. **92**, 151911 (2008).

[14] A. A. Balandin, S. Ghosh, W. Bao, I. Calizo, D. Teweldebrhan, F. Miao, and C. N. Lau, Superior thermal conductivity of single-layer graphene, Nano Lett. **8**, 902 (2008).

[15] Q. H. Wang, K. Kalantar-Zadeh, A. Kis, J. N. Coleman, and M. S. Strano, Electronics and optoelectronics of two-dimensional transition metal dichalcogenides, Nat. Nanotech. **7**, 699 (2012).

[16] M. Xu, T. Liang, M. Shi, and H. Chen, Graphene-like two-dimensional materials, Chem. Rev. **113**, 3766 (2013).

[17] K. F. Mak, C. Lee, J. Hone, J. Shan, and T. F. Heinz, Atomically Thin MoS$_2$: A new Direct-Gap Semiconductor, Phys. Rev. Lett. **105**, 136805 (2010).

[18] E. Pop, Energy dissipation and transport in nanoscale devices, Nano Res. **3**, 147 (2010).

[19] M. Fukuda, *Reliability and Degradation of Semiconductor Lasers and LEDs* (Artech House, Boston, 1991).

[20] Z. Yan, G. Liu, J. M. Khan, and A. A. Balandin, Graphene quilts for thermal management of high-power GaN transistors, Nat. Commun. **3**, 827 (2012).

[21] A. C. Neto, F. Guinea, N. M. Peres, K. S. Novoselov, and A. K. Geim, The electronic properties of graphene, Rev. Mod. Phys. **81**, 109 (2009).

[22] S. Bertolazzi, D. Krasnozhon, and A. Kis, Nonvolatile memory cells based on MoS$_2$/graphene heterostructures, ACS Nano **7**, 3246 (2013).

[23] T. Georgiou, R. Jalil, B. D. Belle, L. Britnell, R. V. Gorbachev, S. V. Morozov, Y.-J. Kim, A. Gholinia, S. J. Haigh, O. Makarovsky *et al.*, Vertical field-effect transistor based on graphene–WS$_2$ heterostructures for flexible and transparent electronics, Nat. Nanotech. **8**, 100 (2013).

[24] L. Li, Y. Yu, G. J. Ye, Q. Ge, X. Ou, H. Wu, D. Feng, X. H. Chen, and Y. Zhang, Black phosphorus field-effect transistors, Nat. Nanotech. **9**, 372 (2014).

[25] A. Sood, F. Xiong, S. Chen, H. Wang, D. Selli, J. Zhang, C. J. McClellan, J. Sun, D. Donadio, Y. Cui, E. Pop, and K. E. Goodson, An electrochemical thermal transistor, Nat. Commun. **9**, 4510 (2018).

[26] A. Sood, F. Xiong, S. Chen, H. Wang, D. Selli, J. Zhang, C. J. McClellan, J. Sun, D. Donadio, Y. Cui, E. Pop, and K. E. Goodson, An electrochemical thermal transistor, Nat. Commun. **9**, 4510 (2018).

[27] T.-K. Hsiao, H.-K. Chang, S.-C. Liou, M.-W. Chu, S.-C. Lee, and C.-W. Chang, Observation of room-temperature ballistic thermal conduction persisting over 8.3 μm in SiGe nanowires, Nat. Nanotechnol. **8**, 534 (2013).

[28] V. Lee, C.-H. Wu, Z.-X. Lou, W.-L. Lee, and C.-W. Chang, Divergent and Ultrahigh Thermal Conductivity in Millimeter-Long Nanotubes, Phys. Rev. Lett. **118**, 135901 (2017).

[29] A. I. Hochbaum, R. Chen, R. D. Delgado, W. Liang, E. C. Garnett, M. Najarian, A. Majumdar, and P. Yang, Enhanced thermoelectric performance of rough silicon nanowires, Nature **451**, 163 (2008).

[30] S. Neogi, J. S. Reparaz, L. F. C. Pereira, B. Graczykowski, M. R. Wagner, M. Sledzinska, A. Shchepetov, M. Prunnila, J. Ahopelto, C. M. Sotomayor-Torres, *et al.*, Tuning thermal transport in ultrathin silicon membranes by surface nanoscale engineering, ACS Nano **9**, 3820 (2015).

[31] S. Lee, F. Yang, J. Suh, S. Yang, Y. Lee, G. Li, H. S. Choe, A. Suslu, Y. Chen, and C. Ko *et al.*, Anisotropic in-plane thermal conductivity of black phosphorus nanoribbons at

temperatures higher than 100 k, Nat. Commun. **6,** 8573 (2015).

[32] A. Jain and A. J. McGaughey, Strongly anisotropic in-plane thermal transport in single-layer black phosphorene, Sci. Rep. **5,** 8501 (2015).

[33] G. Liu, H. Wang, Y. Gao, J. Zhou, and H. Wang, Anisotropic intrinsic lattice thermal conductivity of borophane from first-principles calculations, Phys. Chem. Chem. Phys. **19,** 2843 (2017).

[34] M. Zeraati, S. M. Vaez Allaei, I. Abdolhosseini Sarsari, M. Pourfath, and D. Donadio, Highly anisotropic thermal conductivity of arsenene: An ab initio study, Phys. Rev. B **93,** 085424 (2016).

[35] Y. Zhou, Z.-X. Guo, S.-Y. Chen, H.-J. Xiang, and X.-G. Gong, Anisotropic in-plane thermal conductivity in multilayer silicene, Phys. Lett. A **382,** 1499 (2018).

[36] G. A. Slack, Anisotropic thermal conductivity of pyrolytic graphite, Phys. Rev. **127,** 694 (1962).

[37] S. Chen, A. Sood, E. Pop, K. E. Goodson, and D. Donadio, Strongly tunable anisotropic thermal transport in MoS_2 by strain and lithium intercalation: First-principles calculations, 2D Mater. **6,** 025033 (2019).

[38] R. Guo and B. Huang, Thermal transport in nanoporous Si: Anisotropy and junction effects, Int. J. Heat. Mass. Transf. **77,** 131 (2014).

[39] D. Donadio and G. Galli, Atomistic Simulations of Heat Transport in Silicon Nanowires, Phys. Rev. Lett. **102,** 195901 (2009).

[40] J. Lim, K. Hippalgaonkar, S. C. Andrews, A. Majumdar, and P. Yang, Quantifying surface roughness effects on phonon transport in silicon nanowires, Nano Lett. **12,** 2475 (2012).

[41] S. Xiong, K. Sääskilahti, Y. A. Kosevich, H. Han, D. Donadio, and S. Volz, Blocking Phonon Transport by Structural Resonances in Alloy-Based Nanophononic Metamaterials Leads to Ultralow Thermal Conductivity, Phys. Rev. Lett. **117,** 025503 (2016).

[42] B. L. Davis and M. I. Hussein, Nanophononic Metamaterial: Thermal Conductivity Reduction by Local Resonance, Phys. Rev. Lett. **112,** 055505 (2014).

[43] S. Neogi and D. Donadio, Thermal transport in freestanding silicon membranes: Influence of dimensional reduction and surface nanostructures, Eur. Phys. J. B **88,** 73 (2015).

[44] S. Xiong, D. Selli, S. Neogi, and D. Donadio, Native surface oxide turns alloyed silicon membranes into nanophononic metamaterials with ultralow thermal conductivity, Phys. Rev. B **95,** 180301 (2017).

[45] H. Honarvar, L. Yang, and M. I. Hussein, Thermal transport size effects in silicon membranes featuring nanopillars as local resonators, Appl. Phys. Lett. **108,** 263101 (2016).

[46] H. Honarvar and M. I. Hussein, Two orders of magnitude reduction in silicon membrane thermal conductivity by resonance hybridizations, Phys. Rev. B **97,** 195413 (2018).

[47] T. Zushi, K. Ohmori, K. Yamada, and T. Watanabe, Effect of a SiO_2 layer on the thermal transport properties of $\langle 100 \rangle$ Si nanowires: A molecular dynamics study, Phys. Rev. B **91,** 115308 (2015).

[48] C. Mangold, S. Neogi, and D. Donadio, Optimal thickness of silicon membranes to achieve maximum thermoelectric

efficiency: A first principles study, Appl. Phys. Lett. **109,** 053902 (2016).

[49] D. Donadio, Advances in the optimization of silicon-based thermoelectrics: A theory perspective, Curr. Opin. Green Sustainable Chem. **17,** 35 (2019), Novel materials for energy production and storage.

[50] L. Isaeva, G. Barbalinardo, D. Donadio, and S. Baroni, Modeling heat transport in crystals and glasses from a unified lattice-dynamical approach, Nat. Commun. **10,** 3853 (2019).

[51] J. A. Appelbaum, G. Baraff, and D. Hamann, The Si (100) surface. III. Surface reconstruction, Phys. Rev. B **14,** 588 (1976).

[52] J. Tersoff, Modeling solid-state chemistry: Interatomic potentials for multicomponent systems, Phys. Rev. B **39,** 5566 (1989).

[53] In the equilibrium MD simulations, the equations of motion are integrated with a timestep of 0.5 fs to guarantee energy conservation over simulation times of several tens of ns. The initial velocities are set to 300 K and the systems are coupled to a Nosé-Hoover thermostat for 1 ns to decorrelate the systems from the initial configurations. The thermostat is then decoupled from the systems and the heat-flux calculations are performed under microcanonical conditions, and recorded every 5-fs intervals. For every system, κ is estimated by averaging over 10–20 independent runs each with simulation times of 20–30 ns, and the uncertainty is computed from the standard deviation of the independent dataset.

[54] J. Behler and M. Parrinello, Generalized Neural-Network Representation of High-Dimensional Potential-Energy Surfaces, Phys. Rev. Lett. **98,** 146401 (2007).

[55] R. Li, E. Lee, and T. Luo, A unified deep neural network potential capable of predicting thermal conductivity of silicon in different phases, Mater. Today Phys. **12,** 100181 (2020).

[56] Y. He, I. Savić, D. Donadio, and G. Galli, Lattice thermal conductivity of semiconducting bulk materials: Atomistic simulations, Phys. Chem. Chem. Phys. **14,** 16209 (2012).

[57] S. Plimpton, Fast parallel algorithms for short-range molecular dynamics, J. Comput. Phys. **117,** 1 (1995).

[58] R. Zwanzig, Time-correlation functions and transport coefficients in statistical mechanics, Annu. Rev. Phys. Chem. **16,** 67 (1965).

[59] P. K. Schelling, S. R. Phillpot, and P. Keblinski, Comparison of atomic-level simulation methods for computing thermal conductivity, Phys. Rev. B **65,** 517 (2002).

[60] Z. Fan, L. F. C. Pereira, H.-Q. Wang, J.-C. Zheng, D. Donadio, and A. Harju, Force and heat current formulas for many-body potentials in molecular dynamics simulations with applications to thermal conductivity calculations, Phys. Rev. B **92,** 3689 (2015).

[61] P. B. Allen and J. L. Feldman, Thermal conductivity of disordered harmonic solids, Phys. Rev. B **48,** 12581 (1993).

[62] G. P. Srivastava, *The Physics of Phonons* (Taylor and Francis Group, LLC, New York, NY, 1990).

[63] H. Honarvar and M. I. Hussein, Spectral energy analysis of locally resonant nanophononic metamaterials by molecular simulations, Phys. Rev. B **93,** 081412 (2016).

[64] K. L. Koshelev and A. A. Bogdanov, Interplay between anisotropy and spatial dispersion in metamaterial waveguides, Phys. Rev. B **94**, 115439 (2016).

[65] See Supplemental Material at http://link.aps.org/supplemental/10.1103/PhysRevApplied.14.024004 for computational method details and additional supporting results.

[66] P. G. Klemens, The scattering of low-frequency lattice waves by static imperfections, Procs. Phys. Soc. A **68**, 1113 (1955).

[67] L. Lindsay and D. A. Broido, Three-phonon phase space and lattice thermal conductivity in semiconductors, J. Phys.: Condens. Matter **20**, 165209 (2008).

[68] P. B. Allen, J. L. Feldman, J. Fabian, and F. Wooten, Diffusons, locons and propagons: Character of atomie yibrations in amorphous Si, Philos. Mag. B **79**, 1715 (1999).

[69] T. Zhu and E. Ertekin, Phonons, localization, and thermal conductivity of diamond nanothreads and amorphous graphene, Nano Lett. **16**, 4763 (2016).

[70] M. N. Luckyanova, J. Mendoza, H. Lu, B. Song, S. Huang, J. Zhou, M. Li, Y. Dong, H. Zhou, and J. Garlow, Phonon localization in heat conduction *et al.*, Sci. Adv. **4**, eaat9460 (2018).

[71] S. Hu, Z. Zhang, P. Jiang, J. Chen, S. Volz, M. Nomura, and B. Li, Randomness-induced phonon localization in graphene heat conduction, J. Phys. Chem. Lett. **9**, 3959 (2018).

[72] S. Hu, Z. Zhang, P. Jiang, W. Ren, C. Yu, J. Shiomi, and J. Chen, Disorder limits the coherent phonon transport in two-dimensional phononic crystal structure, Nanoscale **11**, 11839 (2019).

[73] T. Juntunen, O. Vänskä, and I. Tittonen, Anderson Localization Quenches Thermal Transport in Aperiodic Superlattices, Phys. Rev. Lett. **122**, 105901 (2019).

[74] J. L. Feldman, M. D. Kluge, P. B. Allen, and F. Wooten, Thermal conductivity and localization in glasses: Numerical study of a model of amorphous silicon, Phys. Rev. B **48**, 12589 (1993).

[75] J. L. Feldman, P. B. Allen, and S. R. Bickham, Numerical study of low-frequency vibrations in amorphous silicon, Phys. Rev. B **59**, 3551 (1999).

[76] N. Chekurov, K. Grigoras, A. Peltonen, S. Franssila, and I. Tittonen, The fabrication of silicon nanostructures by local gallium implantation and cryogenic deep reactive ion etching, Nanotechnol. **20**, 065307 (2009).

[77] Z. Huang, X. Zhang, M. Reiche, L. Liu, W. Lee, T. Shimizu, S. Senz, and U. Gösele, Extended arrays of vertically aligned sub-10 nm diameter [100] Si nanowires by metal-assisted chemical etching, Nano Lett. **8**, 3046 (2008).

[78] M. J. Bierman, Y. A. Lau, A. V. Kvit, A. L. Schmitt, and S. Jin, Dislocation-driven nanowire growth and eshelby twist, Science **320**, 1060 (2008).

[79] K. A. Dick, K. Deppert, M. W. Larsson, T. Mårtensson, W. Seifert, L. R. Wallenberg, and L. Samuelson, Synthesis of branched 'nanotrees' by controlled seeding of multiple branching events, Nat. Mater. **3**, 380 (2004).

[80] Y. Jung, D.-K. Ko, and R. Agarwal, Synthesis and structural characterization of single-crystalline branched nanowire heterostructures, Nano Lett. **7**, 264 (2007).